Sensor response estimate and cross calibration of paleomagnetic measurements on pass-through superconducting rock magnetometers

Chuang Xuan [1, *] and Hirokuni Oda [2]

[1] School of Ocean and Earth Science, National Oceanography Centre Southampton, University of Southampton, Waterfront Campus, European Way, Southampton, SO14 3ZH, UK

[2] Research Institute of Geology and Geoinformation, Geological Survey of Japan, AIST, Central 7, 1-1-1 Higashi, Tsukuba 305-8567, Japan

[*] Corresponding Author: Chuang Xuan (C.Xuan@soton.ac.uk)

Key Points

- We present a software for accurate estimate of magnetometer sensor response needed for reliable deconvolution of paleomagnetic measurements
- Normalization using a nine-term matrix calculated from sensor response estimate reduces discrepancies between data from two magnetometers
- Deconvolution restores consistent and high-resolution data from measurements of a sample on two magnetometers with distinct sensor responses

Abstract

Pass-through superconducting rock magnetometers (SRMs) enable rapid and precise remanence measurement of continuous samples and are essential for paleomagnetic studies. Due to convolution effect of the SRM sensor response, pass-through measurements need to be deconvolved to restore accurate and high-resolution signal. A key step towards successful deconvolution is a reliable estimate of the SRM sensor response. Here, we present new tool URESPONSE for accurate SRM sensor response estimate based on measurements of a well-calibrated magnetic point source (MPS). URESONSE allows sensor response to be estimated for continuous samples with different cross-section geometry. We estimate sensor responses for an old liquid-helium-cooled SRM (SRM-old) and a new liquid-helium-free SRM (SRM-new) at University of Southampton, and compare remanence measurement of a u-channel on both SRMs before and after deconvolution. For each SRM, sensor response estimates based on data collected using different MPS samples and/or measurement procedures generally yield small differences (std. < ~1%), while sensor response estimates for continuous samples with different cross-section geometry often show larger differences (std. up to ~2%). Compared with SRM-old, SRM-new has smaller cross-axis responses, less negative zones, and significantly broader main-axis responses. We demonstrate that normalization of data using a nine-element "effective-length" matrix calculated from sensor response estimate is necessary to minimize differences in measurements on two SRMs. Deconvolution of measurements on two SRMs using accurate sensor response estimates yields highly consistent and high-resolution results, while deconvolution using inaccurate sensor response data can lead to significant differences especially for data from SRM-old that has large cross-axis responses.

Keywords: superconducting rock magnetometer; deconvolution; sensor response estimate; u-channel sample; magnetic point source; paleomagnetism

Plain Language Summary

Pass-through superconducting rock magnetometer is one of the most versatile tools for measuring magnetic signals preserved in rocks, sediments and other materials. It allows long samples to be measured continuously at high speed and has greatly contributed to paleomagnetic and environmental magnetic studies. Data acquired on these magnetometers are smoothed and distorted because of the way the magnetometer's sensors respond to signal carried by the sample. To overcome these effects, we developed a software to estimate how the magnetometers' sensors respond to sample signal in 3D space. The software reads measurement data collected using a small volume sample with known stable magnetic signal, and uses the data to calculate the magnetometer's response to samples with different shape. The sensors of two different magnetometers appear to respond to signal carried by the same sample in distinct ways, and measurements of the same sample on the two magnetometers show significant differences. A simple correction using factors calculated by the software can largely reduce these differences. We also show that estimates of the magnetometer's sensor responses produced by the software can be used to restore detailed and consistent magnetic signals through inverse calculation.

1. Introduction

The development of pass-through superconducting rock magnetometers (SRM) has allowed high-sensitivity and rapid measurement of remanent magnetizations in continuous rock and sediment samples (e.g., Dodson et al., 1974; Weeks et al., 1993). The large volume of continuous records acquired on SRMs using u-channel samples (Tauxe et al., 1983) have greatly contributed to paleomagnetism and environmental magnetism studies (e.g., Channell et al., 2009; Roberts et al., 2013). These records represent one of the most important data archive in the building of paleomagnetic databases (e.g., Brown et al., 2015) and provide valuable constraints on time and spatial varying geomagnetic field models (e.g., Korte et al., 2011; Nilsson et al. 2014). However, continuous measurements on pass-through SRMs are smoothed and distorted due to convolution effect of the SRM's sensor response (e.g., Roberts 2006; Philippe et al., 2018), and it is desirable to perform deconvolution as a routine for processing pass-through paleomagnetic data to restore accurate and high-resolution remanent magnetization signal.

Various algorithms have been proposed to deconvolve continuous paleomagnetic data acquired on pass-through SRMs (e.g., Dodson et al., 1974; Constable & Parker, 1991; Oda & Shibuya, 1996; Jackson et al. 2010). Jackson et al. (2010) compared deconvolution results estimated using singular value decomposition and regularized least squares with those estimated using the Akaike's Bayesian Information Criterion (ABIC) minimization-based method (Oda & Shibuya, 1996), and demonstrated that if the SRM sensor response is accurately estimated the three methods recover consistent and high-resolution magnetization signal. Building on the ABIC-minimization based method, Oda and Xuan (2014) developed an improved deconvolution algorithm that considers realistic uncertainties in sample length and measurement position. The new algorithm is implemented in the UDECON software (Xuan & Oda, 2015), which allows the users to directly read measurement files produced by

pass-through SRMs and perform optimized deconvolution. Yamamoto et al. (2018) used UDECON together with a recent sensor response estimate of the SRM at Kochi Core Center (Oda et al., 2016) to demonstrate that deconvolution can restore detailed magnetization direction and intensity signal comparable to those measured using back-to-back discrete samples, supporting the results of experiments conducted by Guyodo et al. (2002) that compared deconvolved u-channel data with measurements of discrete samples cut from the u-channel.

A key step towards successful deconvolution is to obtain an accurate estimate of the SRM's sensor response for a continuous paleomagnetic sample. SRM sensor response is defined by the geometry of pick-up coils and superconducting shield as well as the shape of the paleomagnetic samples (e.g., Shibuya & Michikawa, 2000; Jackson et al., 2010; Oda & Xuan, 2014). For example, Lascu et al. (2012) conducted deconvolution experiments on pass-through data collected on continuous cement samples with different cross sections and concluded that it is important to perform deconvolution using SRM response function tailored specifically for the shape of the sample. Estimation of SRM sensor response often involves repeated pass-through measurements of a very thin test sample (Constable & Parker, 1991), sheets of magnetic tape (Oda & Shibuya, 1996), a short-length magnetic tape mounted in a glass tube (Parker & Gee, 2002), or a synthetic cube sample (Jackson et al., 2010). To avoid potential issue caused by sample inhomogeneity and/or varying procedures for sensor response estimate of different axes, Oda and Xuan (2014) introduced magnetic point source (MPS) sample held in the center of a small cube with six faces parallel or orthogonal to the magnetic moment direction of the MPS to collect measurement data for SRM sensor response estimate. The MPS sample can be repeatedly measured while it is precisely placed at different positions on cross-section orienting parallel/antiparallel to each of the three SRM

axes. This method was used to estimate sensor response of the SRMs at the Oregon State University (Oda & Xuan, 2014) and the Kochi Core Center (Oda et al., 2016).

SRM measurements of an MPS sample produce a rich set of data making it possible to accurately estimate SRM sensor response for pass-through measurements collected at different resolution and for paleomagnetic samples with various shape. However, there is currently no algorithm/tool available to facilitate the optimization of SRM sensor response estimate. In this study, we first develop a new software URESPONSE with easy-to-use graphical user interface to process MPS data and make accurate and customized SRM sensor response estimates for paleomagnetic sample measurements in preparation for reliable deconvolution in UDECON. The software is then used to estimate and compare sensor responses of two types of 2G-Enterprises pass-through SRMs available at the University of Southampton. We compare measurements of a u-channel sample collected on both SRMs and discuss cross-calibration and improved normalization method needed to reduce discrepancies in paleomagnetic data acquired on different SRMs. We also demonstrate that deconvolution of paleomagnetic data measured on different SRMs using accurate SRM sensor response estimates produce highly consistent and high-resolution results.

2. Samples and Methods

2.1 Magnetic point source samples and measurements

University of Southampton (UoS) houses two generations of 2G Enterprises pass-through superconducting rock magnetometers (SRMs) in a magnetically shielded room (Figure 1a): an old liquid-helium cooled SRM and a new liquid-helium free SRM (hereinafter referred to

as SRM-old and SRM-new, respectively). SRM-old was originally installed in 1991 with radio frequency (RF) superconducting quantum interference devices (SQUID) and a large sample access bore (7.6 cm diameter), and was upgraded in 2001 with direct current (DC) SQUID and a narrow sample access bore (4.2 cm diameter). SRM-new was installed in September 2017 and is equipped with a pulse tube cryocooler that operates completely liquid-helium free. SRM-new is equipped with DC SQUID and a narrow sample access bore (4.2 cm diameter). The three orthogonal measurement axes of both SRMs have been configured so that when viewed from the side with the sample load/unload zone on the right, the +X, +Y and +Z axes point vertically down, horizontally away, and horizontally to the right, respectively (Figure 1b).

Two magnetic point source (MPS) samples (i.e. MPS-2 and MPS-11 created in 2011 and 2015, respectively) were used in this study for sensor response estimate of the SRMs at UoS. MPS-2 and MPS-11 were previously used for sensor response estimates of SRMs at the Oregon State University (Oda & Xuan, 2014) and the Kochi Core Center (Oda et al., 2016), respectively. Both MPS samples were made using plastic magnet powders (Hc = 890 mT, Hcr = 894 mT) and instant glue. For MPS-2, a 2.5-T pulse magnetic field was applied three times while the instant glue was hardening (Oda & Xuan, 2014). For MPS-11, static magnet with a peak magnetic field of 1.4 T was applied for ~10 seconds while the instant glue was hardening. Both MPS samples were subsequently demagnetized using alternating field (AF) with a peak field of 50 mT. The MPS samples are enclosed in the center of a plastic cube with 5 mm edge length, and carry a stable remanent magnetization perpendicular to one surface of the cube (Figure 1c). Magnetic moment of the two MPS samples has been monitored through time on an ASPIN-2 spinner magnetometer (Natsuhara Giken Co. Ltd.) at the National Institute of Advanced Industrial Science and Technology (AIST) in Japan

(Figure 2, Tables S1 and S2). A well-shaped holder was used to ensure accurate orientation of MPS-11 magnetic moment during spinner magnetometer measurement (see Figure S1).

We conducted multiple sets of MPS measurements on both SRMs at UoS between December 2013 and March 2018. Each set of MPS measurements involves measuring the MPS at high-resolution (i.e. 1 to 10 mm spacing) over the possible sensor response range along the SRM Z-axis (typically about 40-50 cm). MPS is repeatedly measured while it is placed at different grid positions on the X-Y cross-section plane orienting parallel or antiparallel to each of the three SRM axes (Figures 1b-c). A cubic plastic block with 25 mm edge length and 5×5 or 4×4 grids marked or carved on one surface is used to hold the MPS at different positions on the X-Y cross-section (Figure 1c). Grid positions on the block with 5×5 grids are evenly distributed with 5 mm × 5 mm spacing and orientation of the MPS cube at each grid position is controlled by a plastic rod (Oda & Xuan, 2014). Grid positions on the block with 4×4 grids are evenly distributed with 6 mm × 6 mm spacing and MPS cube orientation at each grid position is constrained by precisely carved plastic walls on four sides (Oda et al., 2016). Four (three) sets of MPS measurements were collected on SRM-old (SRM-new). These measurements used various combinations of MPS sample, measurement resolution, and cross-section grids (see Table 1). MPS-2 was used for measurements on SRM-old in Dec 2013, and all the rest of MPS measurements for this study were collected using MPS-11. Note that for MPS-11 measurements made on SRM-new in Sept. 2017, SRM-new X-axis measurements experienced drifting issues and hence X-axis data from those measurements are not used for analysis in this study.

2.2 New algorithm for SRM sensor response estimate

To estimate each of the nine SRM sensor response terms (i.e. XX, XY, XZ, YX, YY, YZ, ZX, ZY, ZZ; where in each term the first letter denotes orientation of the MPS and the second letter denotes the SRM pick-up coil), MPS measurements of that term for all cross-section grid positions at each measurement interval (along the Z axis) are usually interpolated using a 2D spline function at high resolution (e.g. every 1 mm^2) and then integrated over the cross-section area of pass-through samples (Oda & Xuan, 2014; Xuan & Oda 2015; Oda et al., 2016). In this study, we process all measurement data related to each response term as 3D matrix, and use 3D spline interpolation (e.g. at 1 mm^3 resolution) followed by 3D integration to estimate SRM sensor response. The 3D interpolation approach is more robust than 2D interpolation at each measurement position as it considers links between nearby measurement positions, and would have better performance especially considering positioning errors of the SRM tracking system (e.g. Oda et al., 2016). By integrating the interpolated data over different 3D volumes, the new approach allows SRM sensor response to be estimated at different resolution along the Z-axis and for continuous samples with different rectangular shape and/or center position on cross section (Figure 3). We incorporate the new algorithm in MATLAB (version 2018a) program and develop easy-to-use software with graphical user interface to conveniently estimate SRM sensor response for different scenarios based on MPS measurements (Figure 4).

2.3 Test u-channel measurements and deconvolution

To investigate how sensor response of different SRMs influence measurements of the same sample and test if deconvolution using varying sensor response estimates can restore consistent and high-resolution signal, we repeatedly measured a u-channel sample on the two SRMs at UoS. The u-channel sample was taken from the archive-half of Core-section

U1438B-3H-2A recovered during International Ocean Discovery Program (IODP) Expedition 351 to the western Pacific (Arculus et al., 2015). The u-channel sample is 1.5m long with an inner cross section of ~1.9 cm (height) by ~1.8 cm (width), and mainly comprises light olive gray mud and moderate yellowish-brown mud. The sample recorded a geomagnetic polarity transition corresponding to top of the Jaramillo subchron (~0.99 Ma). The u-channel sample was AF demagnetized with peak fields of 45 mT, and natural remanence of the sample was repeatedly measured for ten times on SRM-old. The sample is then immediately transferred and repeatedly measured for ten times on SRM-new. All measurements were collected at 1-cm resolution over the sample length as well as over a 10-cm 'leader' interval before the sample and a 10-cm 'trailer' interval after the sample. For deconvolution test, we used the UDECON software (Xuan & Oda, 2015) and various sensor response estimates calculated using the new algorithm to optimize and compare deconvolution of the measurements made on the two SRMs.

3. Results and Discussions

3.1 The URESPONSE software

We have developed a MATLAB program URESPONSE with graphical user interface (GUI) to conveniently estimate SRM sensor response using the new algorithm based on repeated measurements of an MPS sample. URESPONSE generates SRM sensor response data files that can be directly read and used in the UDECON software (Xuan & Oda, 2015) for optimized deconvolution. URESPONSE reads an Excel file that summarizes necessary information about the MPS measurements, and allows users to conveniently view and compare the MPS data (Figure 4a). The Excel summary file, a measurement data format file

same as that described by Xuan and Oda (2015) for the UDECON software, and a folder containing all MPS measurement data files should be placed in the same folder. Measurement of the MPS sample while it is placed at different grid positions on cross-section orienting towards different SRM measurement axes should be stored in separate files. MPS measurement data are labeled and organized on the top right 'Measurement' panel in URESPONSE according to grid position on cross-section and MPS orientation (Figure 4a). All grid positions are plotted on the middle right 'Grids' panel based on their coordinates on the X-Y cross-section plane. Users can choose to view individual or any combination of MPS data associated with different grid positions and/or MPS orientations by selecting corresponding label(s) on the 'Measurement' panel (Figure 4a). Selected grid positions are highlighted on the 'Grids' panel. Users can also choose to show MPS data measured along any combination of the SRM measurement axes using checkboxes located in the 'Terms' panel on the bottom right of the software.

The 'Response Estimate Parameters' panel on the bottom of URESPONSE (Figure 4b) includes parameters that can be adjusted for SRM sensor response estimate. These parameters define the resolution of 3D interpolation for each of the nine response terms and 3D volumes (see Figure 3) for subsequent integration of the interpolated data that correspond to paleomagnetic sample geometry and measurement intervals. The 'On cross section' and 'Along the track' boxes define resolution of the 3D interpolation grids on the cross-section and along the track, respectively. The 'Cross-section center offset (cm)' and 'Integration volume dimension (cm)' boxes define the volume over which the 3D integration is done for SRM sensor response estimates. Values in the 'Height' and 'Width' boxes are used to define the cross-section shape of the volume occupied by a paleomagnetic sample, and value in the 'Length' box defines length of the 3D integration volume along the track and should match

the actual measurement interval of paleomagnetic sample along the track. ‘Horizontal’ and ‘Vertical’ offset values are used to quantify difference in center positions between the paleomagnetic sample and the MPS measurement grids on cross-section. Radio buttons are provided to choose between two options for normalization of the integrated raw sensor response: (1) absolute magnetic moment of the MPS sample if provided in the Excel summary file; or (2) the average of the maximum response value of the XX and YY terms.

When all ‘Response Estimate Parameters’ are set, users can press the ‘Calculate SRM Response’ button to generate a sensor response estimate (Figure 4b). Note that as the ZZ response term often show double peaks, the center position of the calculated SRM sensor response along the Z-axis is determined by averaging the maximum response positions of the XX and YY terms. Comparison of the estimated and user measured MPS position is displayed on the upper left corner below nine EL values providing information on if measurement positions of the SRM are properly calibrated. Users can view either the integrated raw or normalized sensor response using the ‘Show Normalized Response’ checkbox beneath the ‘Response’ panel. Cross section area of the volume used for response estimate is shown as a red rectangle on the ‘Grids’ panel along with interpolated grid points shown as small black dots. Checkboxes on the ‘Terms’ panel can be used to view any combination of the nine response terms. Users can generate multiple versions of response estimates and different response estimate can be viewed by selecting corresponding label on the ‘Response’ panel. When selected, any terms checked on the ‘Terms’ panel are shown in the main plot area, and parameters used for the response estimate are shown in relevant boxes on the ‘Response Estimate Parameters’ panel (Figure 4b). To export any of the normalized response estimate data as a tab-delimited text file, users can select corresponding estimate on the ‘Response’ panel and click the second icon in the toolbar located on the top left. The

exported file can be directly read by the UDECON software (Xuan and Oda, 2015) as 'response file' and used for optimized deconvolution.

3.2 Cross calibration of the MPS samples and SRMs

In order to compare and calibrate measurements made on different SRMs, MPS samples used for sensor response estimates should: (1) have magnetization direction precisely perpendicular to one surface of the well-shaped small cube containing the MPS; and (2) have their absolute magnetic moment values well estimated and monitored over time. Magnetic moment directions of MPS-11 measured on spinner magnetometer at AIST show average deviation of ~0.5° from the expected direction perpendicular to the MPS cube surface (Table S1). For MPS-2, average deviation of the magnetic moment directions is ~3° (Table S2).

Magnetic moment values of MPS-11 monitored on spinner magnetometer at AIST are shown in Figure 2a. Note that values shown have been corrected using sensitivity factor of the spinner magnetometer calculated based on measurements of a reliable standard sample (see Table S1). Changes in the magnetic moment of MPS-11 are generally small (maximum ~3%) with majority of the changes happen within the first about two years, after which MPS-11 appears to have reached equilibrium and remained stable (changes <~0.1%). MPS-11 magnetic moment values fit well with a sigmoidal curve (red dotted line in Figure 2a). Estimated magnetic moment values of MPS-11 on dates when it was measured on SRM-old or SRM-new for this study, i.e. Jan. 2016, Oct. 2017, and Mar. 2018 (vertical dashed lines in Figure 2), were 5.300×10^{-4} emu, 5.244×10^{-4} emu and 5.244×10^{-4} emu, respectively. MPS-2 was measured at AIST on an SMM-85 spinner magnetometer in Jun. 2011, and then on an ASPIN-2 spinner magnetometer in Dec. 2013 (Table S2). We translate the SMM-85

measurement of 6.012×10^{-3} emu to a predicted ASPIN-2 measurement of 6.174×10^{-3} emu, based on a conversion factor of 1.027 estimated using measurements of other MPS samples on both spinner magnetometers (see details in Table S2). The sensitivity corrected magnetic moment value of 5.937×10^{-3} emu was acquired for MPS-2 on ASPIN-2 in Dec. 2013 around the time when the first two sets of MPS measurements on SRM-old were conducted (i.e. SRM-old_Est1 and SRM-old_Est2). The new ASPIN-2 measurement of MPS-2 suggests an ~3.8% decay in ~30 months since it was created in June 2011.

In Figure 2, magnetic moment of MPS samples measured on SRM-old and SRM-new are shown as red and blue circles, respectively. These values are calculated by averaging peak values in XX, YY, and ZZ terms after integrating 3D-interpolated data (using 0.5×0.5×0.5 mm^3 grids) over a 1×1×1-cm^3 volume with cross-section centered in that of a u-channel (see Table S4 for comparisons of values calculated by integration over volumes of 0.5×0.5×0.5 mm^3, 1×1×1 cm^3, and 2×2×2 cm^3 for the two SRMs). MPS magnetic moment values acquired on SRM-new are close to those measured using the spinner magnetometer with deviations of ~0.25%, whereas values acquired on SRM-old show consistent deviations of ~2.5% compared with those measured using spinner magnetometer (Figure 2b). Smaller deviations on SRM-new could be related to a better calibration by the manufacturer due to the recent installation in 2017 and relatively wider flat sensor response in the center. The larger deviations on SRM-old could be due to calibration of SRM-old at the time of installation. Although 1×1×1-cm^3 volume used for integration in our estimate of magnetic moment values of MPS samples should be comparable to that of a calibration coil, the measurements with a calibration coil could have been influenced by sharper changes due to narrower sensor response of SRM-old and possible offsets from the center of the pick-up coils.

351

352 *3.3 Sensor response estimates of the two SRMs at University of Southampton*

353

354 We used URESPONSE to process each set of MPS measurements listed in Table 1 and create
355 sensor response estimates for the two SRMs at UoS. Default values of 'Response Estimate
356 Parameters' in URESPONSE are used for results shown in Figure 5 (i.e. 'Horizontal' and
357 'Vertical' offsets of 0 cm and 0.1 cm, and 'Height', 'Width' and 'Length' of 1.9 cm, 1.8 cm
358 and 1 cm, respectively). Results shown in Figure 5 are normalized using average of the
359 maximum values in XX and YY terms. For MPS-11 measurements conducted on both SRMs
360 in October 2017 using the same setting (see Table 1), we also calculated response estimates
361 (Figures 6a&d) that are normalized using the MPS-11 magnetic moment value (i.e. 5.244×10^{-4}
362 emu). In addition, we calculated response estimates that simulate two cases of u-channel
363 sample measurements (Figures 6b-c, e-f): a partially filled sample (i.e. by setting 'Height'
364 value and 'Vertical' offset to 1 cm and 0.55 cm respectively), and a sample placed with a
365 horizontal offset of 2 mm towards the -Y direction (i.e. by setting 'Horizontal' offset to -0.2
366 cm).

367

368 For each response estimate in Figure 5, we calculated full widths at half maximum (FWHM)
369 for the main-axis response terms (i.e. XX, YY, and ZZ) which define the main character of
370 the sensor response geometry. FWHM values of SRM-old range between 4.49-4.54 cm for X
371 axis (average 4.52 cm), 4.53-4.56 cm for Y axis (average 4.55 cm), and 5.33-5.41 cm for Z
372 axis (average 5.37 cm). FWHM values of SRM-new range between 7.89-7.92 cm for X axis
373 (average 7.91 cm), 7.64-7.72cm for Y axis (average 7.68 cm), and 7.43-7.50 cm for Z axis
374 (average 7.46 cm). In general, differences in estimated FWHM values for each main-axis
375 response term are <0.1 cm. FWHM values of SRM-new are significantly larger (~2.1-3.4 cm)

than those of SRM-old. FWHM values of SRM-new for the three axes are comparable with one another (difference < 0.5 cm). Whereas, FWHM values of SRM-old in Z-axis are significantly larger (~0.8 cm) than those in X- or Y-axis.

We also calculated effective length (EL) for each main-axis response term (Figure 5). EL is estimated by calculating the area under each of the normalized main-axis response curves, and used together with sample cross-section area to calculate volume normalized magnetizations for SRM measurements. For each SRM, different response estimates yielded comparable EL values (differences < ~0.1 cm). SRM-old has EL values of ~3.98 cm, ~4.17 cm, and ~6.23 cm for X, Y, and Z axis, respectively. SRM-new has EL values of ~7.65 cm, ~7.44 cm, and ~7.90 cm for X, Y, and Z axis, respectively. EL values of Z-axis for both SRMs (especially SRM-old) are the largest among the three main-axis response terms, partly due to the fact that ZZ term does not have negative parts as a result of its pick-up coil geometry.

Cross-axis response terms are usually <5% for SRM-new (Figures 5e-g). For SRM-old, cross-axis response terms are mostly <15% (Figures 5a-d), but can reach ~30% (i.e. in ZX term). The large ZX term on SRM-old is likely related to position of the X pick-up coil relative to the integrated volume for response estimate. This is supported by the observation that ZX term of MPS measurements on SRM-old increases in amplitude when cross-section grid position of MPS sample moves from the bottom to the top. Significant YX and XY terms on SRM-old could be originated from a rotation of the SRM sample tray plane relative to Y-Z plane defined by the Y and Z pick-up coils. Similar rotation was reported by previous sensor response estimates of SRMs at different laboratories (e.g. Parker & Gee 2002; Roberts 2006; Jackson et al. 2010; Oda & Xuan 2014; Oda et al., 2016).

In Figure 7, we directly compare response estimates for SRM-old (Figure 7a) and SRM-new (Figure 7b) by subtracting response estimates shown in Figures 5 and 6 from SRM-old_Est4 and SRM-new_Est2, respectively. Histograms of corresponding differences in response estimates for SRM-old and SRM-new are shown in Figures 7c&d. Response estimates based on MPS data collected at different times following the same measurement procedure (e.g. SRM-old_Est3 and SRM-old_Est4, and SRM-new_Est3 and SRM-new_Est2; see Table 1) produce very similar results with differences typically <2% and std. of ~0.4% (black curves in Figure 7). For SRM-new, response estimate based on 1-cm resolution MPS measurement (i.e. SRM-new_Est1) show differences up to >5% (e.g. in 'ZY' term) with std. of ~1.1% (dark blue curves in Figure 7b), suggesting higher-resolution MPS measurements (e.g. 2mm) are preferred for accurate sensor response estimate. For SRM-old, response estimates based on 1-mm resolution MPS-2 measurements yield generally comparable results with differences mostly <5% (std. of ~0.7-1%) but reaching 5% around a negative peak of ZX term for SRM-old_Est2 (see dark and light blue curves in Figures 7a&c). These differences could be related to less-well constrained magnetic moment direction of MPS-2 (see Section 3.2).

For both SRMs, response estimates for a partially filled u-channel (see Figures 6b&e) show large deviations from the reference estimates with differences reaching >10% (e.g. in ZY term) and std. of ~1.7-1.9% (red curves in Figure 7). Response estimates for horizontally shifted (e.g. by 2 mm) u-channel (see Figures 6c&f) also show large deviations from the reference estimates with differences reaching >5% (e.g. in ZX term) and std. of ~0.8-1% (green curves in Figure 7). These observations are supported by the histograms of the differences (Figures 7c&d), which show that majority of the difference values are small (i.e.

<~2%) while response estimates for partially filled (red curves in Figures c&d) or horizontally shifted (green curves in Figures c&d) samples yield larger range of differences.

3.4 Comparison of u-channel data measured on two SRMs

Repeated magnetic moment measurements (ten times) of the test u-channel made on the same SRM are highly consistent with one another, and differences between them are barely observable in Figure 8a. However, there are substantial differences between magnetic moments obtained from SRM-old and SRM-new. Magnetic moments obtained from SRM-new are smoother and significantly larger than those from SRM-old due to the generally broader sensor responses that integrate signal over longer intervals of the u-channel (i.e. FWHM and EL are ~2-3 cm longer on SRM-new, see Figure 5).

The default software provided by the SRM manufacturer (2G Enterprises) converts voltage readings on an SRM to magnetic moment in 'emu' using a coefficient in 'emu/volts' for each axis determined based on factory calibration. Magnetic moment ($\boldsymbol{d_i}$ in emu) values are then normalized by sample cross-section area ($\boldsymbol{a}$ in cm^2) and EL of each axis ($\boldsymbol{l_i}$ in cm) to calculate volume normalized magnetizations ($\boldsymbol{m_i}$ in emu/cc), following the formulae below.

$$\boldsymbol{d_i} = \boldsymbol{a} \cdot \boldsymbol{l_i} \cdot \boldsymbol{m_i} \qquad (1),$$

where $\boldsymbol{i}$ represents either X-, Y-, or Z-axis data. We refer to magnetization calculated using formulae (1) as single EL normalized magnetization. Magnetizations of the test u-channel calculated using single EL normalization of repeated magnetic moment measurements on the two SRMs are shown in Figure 8b. Single EL normalized data from the two SRMs appear to

be more comparable than data from the two SRMs before the normalization (Figures 8a&b). Although single EL normalized magnetizations from the two SRMs seem to match well along the Z axis (some differences are related to position shift along the Z-axis), there are significant differences along the X- and Y-axis data from the two SRMs. These differences are likely due to non-negligible cross-axis response terms that are not accounted for by the single EL normalization.

We propose to normalize magnetic moment measurements on SRMs using sample cross-section area and a nine-term EL matrix following formulae (2) below.

$$\begin{bmatrix} \boldsymbol{d_X} \\ \boldsymbol{d_Y} \\ \boldsymbol{d_Z} \end{bmatrix} = \boldsymbol{a} \cdot \begin{bmatrix} \boldsymbol{l_{XX}} & \boldsymbol{l_{YX}} & \boldsymbol{l_{ZX}} \\ \boldsymbol{l_{XY}} & \boldsymbol{l_{YY}} & \boldsymbol{l_{ZY}} \\ \boldsymbol{l_{XZ}} & \boldsymbol{l_{YZ}} & \boldsymbol{l_{ZZ}} \end{bmatrix} \cdot \begin{bmatrix} \boldsymbol{m_X} \\ \boldsymbol{m_Y} \\ \boldsymbol{m_Z} \end{bmatrix} \qquad (2),$$

where $\boldsymbol{l}$ is a tensor with nine components corresponding to effective lengths calculated from each of the nine normalized SRM sensor response terms. This nine-term EL matrix accounts for the fact that each vector component of measured magnetic moment is affected by magnetization along all three axes through SRM sensor response including cross terms. Magnetization $\boldsymbol{m}$ can be calculated by solving formulae (2) with the inverse matrix of $\boldsymbol{l}$. We refer to magnetization calculated using formulae (2) as full EL normalized magnetization. URESPONSE software automatically calculates and displays the nine-term EL matrix on top left region of the main plot (see Figure 4b). Magnetizations of the test u-channel calculated using full EL normalization of repeated magnetic moment measurements on the two SRMs are shown in Figure 8c. It is clear that full EL normalization largely reduces the discrepancies between data acquired on the two SRMs.

We compare declination, inclination, and total magnetization intensity data of the test u-channel acquired on the two SRMs using both single and full EL normalized data in Figure 9. The two normalization methods yield only very minor differences for data acquired on SRM-new. This is probably due to less significant cross-axis response terms and larger FWHM of the main-axis response terms on SRM-new (i.e. EL matrix of SRM-new is dominated by main-axis response contributions with almost negligible contributions from the cross-axis response terms). Declination data acquired on SRM-old using single and full EL normalizations, however, show differences up to ~10° (light and dark gray curves in Figure 9a). This large discrepancy is likely related to large contributions of cross-terms on SRM-old sensor response especially in YX and XY terms (see Figure 4) that are not compensated for by single EL normalization. Declinations acquired on both SRMs using full EL normalized data are more consistent with one another (dark gray and dark blue curves in Figure 9a), compared with those acquired using single EL normalized data (light grey and light blue curves in Figure 9a).

3.5 Comparison of deconvolved u-channel data

Although full EL normalization compensates for differences in SRM sensor responses to some extent and provides a reasonable correction of paleomagnetic data acquired on different SRMs, it is not sufficient to overcome differences or smoothing introduced by sensor responses of different SRMs. A fundamental solution to restore the high-resolution and undistorted signal relies on deconvolution. Deconvolved magnetization data of the u-channel using measurements acquired on SRM-old (SRM-new) and response estimate of SRM-old_Est4_v2 (SRM-new_Est2_v2) normalized using calibrated MPS magnetic moment are shown in Figure 8d. Corresponding declination, inclination, and total magnetization intensity

500 data are compared in Figure 9. Errors associated with the deconvolution of X, Y, and Z data
501 are shown in Figure S2 and are typically two orders of magnitudes lower than the signal.
502
503 Deconvolution results of repeated measurements on the same SRM (ten times) show little
504 difference, suggesting that typical errors associated with the SRM measurements of the
505 sample do not yield significant differences in optimized deconvolution using UDECON if the
506 same accurate sensor response estimate is used. Deconvolved SRM-old and SRM-new data
507 are remarkably similar on all three axes in terms of both amplitudes and detailed variabilities
508 (Figure 8d). In addition, optimized deconvolution using UDECON apparently has also
509 accounted for position shift observable between SRM-old and SRM-new data before
510 deconvolution (Figures 8b&c). Deconvolved paleomagnetic directions and total
511 magnetizations are again highly consistent between SRM-old and SRM-new results (green
512 and red curves in Figure 9), and show clearly repeatable and high-resolution variabilities that
513 are not observed in data before deconvolution. For example, the large swing in inclination at
514 ~50 cm seen in deconvolved data from both SRM-old and SRM-new, was not shown in data
515 before deconvolution. These results suggest that using accurate sensor response estimates
516 generated by URESPONSE, deconvolution can successfully overcome the smoothing and
517 distortion effects induced by the sensor responses of different SRMs.
518
519 For u-channel measurements on each SRM, we also conducted deconvolution using three
520 additional response estimates that simulate: (1) a partially filled u-channel (i.e. SRM-
521 old_Est4_v3 and SRM-new_Est2_v3), (2) u-channel that is placed horizontally shifted (2 mm
522 towards -Y) on the sample tray (i.e. SRM-old_Est4_v4 and SRM-new_Est2_v4), and (3) no
523 cross-axis response terms (i.e. SRM-old_Est4_v2 and SRM-new_Est2_v2 with cross terms
524 set to 0). Corresponding deconvolved data are compared in Figure 10 together with those

deconvolved with sensor response estimates calculated using default URESPONSE parameters (i.e. SRM-old_Est4_v2 and SRM-new_Est2_v2).

Deconvolution of SRM-old data using response estimate without cross-terms (black curves in Figures 10a-c) yield the largest deviations from the reference deconvolution result using SRM-old_Est4_v2 (red curves in Figures 10a-c). The differences are particularly large for X-axis data and for some intervals (e.g. ~40-70 cm) of the Y-axis data. Deconvolution of SRM-old data using response estimates that simulate partially filled (blue curves in Figures 10a-c) or horizontally shifted (green curves in Figures 10a-c) u-channels show smaller but significant deviations from the reference data especially for some intervals of the X- and Y-axis results. These results demonstrate the large contribution of cross-terms in SRM-old measurements and the importance of accurate sensor response estimate for reliable deconvolution of SRM-old data.

Deconvolution of SRM-new data using different response estimates appears to yield generally small differences from the reference deconvolution result using SRM-new_Est2_v2 (red curves in Figures 10d-f). Deconvolution of SRM-new data using different response estimates presented here seems to show smaller deviations in results for Z-axis than those for X- and Y-axis (Figure 10f). Deconvolution of SRM-new data using response estimate without cross-terms (black curve in Figure 10d) or response estimate for horizontally shifted u-channel (green curve in Figure 10d) shows some deviations in X-axis results. Deconvolution using response estimate associated with a partially filled u-channel yields deviations for some intervals in Y-axis results (blue curve in Figure 10e). The fact that sensor response estimates of SRM-new (Figures 4b, 5e-g, and 6d-f) show generally small amplitude cross-terms (i.e. XY, YX, XZ and YZ terms) or have comparable positive and negative areas

in cross-terms (i.e. ZX and ZY terms) could explain why deconvolution using sensor response estimate without cross-terms does not seem to generate significant differences.

4. Conclusions

We present new algorithm and software (URESPONSE) for sensor response estimate of a superconducting rock magnetometer (SRM) based on 3D interpolation and integration of measurement data of well-calibrated magnetic point source (MPS) samples. The new algorithm allows SRM sensor response to be estimated for measurements of samples with different rectangular shapes and/or center position on cross-section, and for pass-through measurements made at different resolutions.

Using multiple sets of MPS measurements and URESPONSE, we compared sensor response of two SRMs at the University of Southampton. MPS magnetic moment obtained from SRM-old and SRM-new measurements show deviations of ~0.25% and ~2.5% from values acquired on well-calibrated spinner magnetometer. Sensor response estimates for each SRM using different sets of MPS measurements yielded small differences (std. < ~1%), but sensor response estimates for the two SRMs show distinct features probably due to differences in the two SRM's pick-up coils configuration and superconducting shields. Compared to SRM-old, SRM-new has significantly broader main-axis responses (~2.1-3.4 cm larger in FWHM), generally less negative regions in main-axis responses, and significantly smaller cross-axis responses. For both SRMs, sensor response estimates for continuous samples with different rectangular shape or center position on cross-section show differences with std. up to ~2%.

Magnetic moment measurements of a test u-channel sample repeatedly collected on the same SRM for ten times are highly consistent with one another, but repeated measurements of the same sample on the two SRMs show significant differences in both magnetization amplitudes and directions. We demonstrate that conventional volume normalization based on a single effective length (EL) value for each measurement axis is inadequate, and normalization using a nine-term EL matrix is necessary to minimize the differences in measurements on different SRMs. The nine-term EL matrix is reported by the URESPONSE software, and should be used to normalize paleomagnetic data acquired on pass-through SRMs.

Deconvolution of the test u-channel measurements on both SRMs using sensor responses estimated based on default URESPONSE parameters successfully restores detailed magnetizations and directional features that are remarkably consistent with one another. Deconvolution of the same data using sensor responses of the two SRMs estimated for samples with different rectangular shape or center position on cross-section, or sensor response without any cross-axis response show significant differences especially for results from SRM-old, suggesting that accurate sensor response estimate is important for reliable deconvolution of pass-through SRM data.

Acknowledgements

The new liquid helium free SRM at Southampton was acquired through support of UK NERC strategic environmental science capital grant CC081. Chuang Xuan is also supported by UK NERC grants NE/R018235/1 and NE/R011281/1. Hirokuni Oda is supported by JSPS KAKENHI Grant Number JP16H04043. We thank Mark Bourne and Tim van Peer for help

599 with the MPS measurements conducted on SRM-old in December 2013, and Yuxi Jin for
600 help with all the rest of the MPS and test u-channel sample measurements on both SRMs at
601 the University of Southampton. Nobuyoshi Natsuhara kindly provided standard samples for
602 spinner magnetometer calibration. We thank Emiko Miyamura and Ayako Katayama for
603 MPS measurements on the spinner magnetometers at AIST. We are also grateful for helpful
604 and constructive comments on the manuscript provided by Valera Shcherbakov and an
605 anonymous reviewer. The URESPONSE software, examples of MPS measurement data files,
606 Excel summary file, measurement data format file, as well as a detailed user's guide of the
607 software can be downloaded using the following link: http://earthref.org/ERDA/2396/.

608 **References**

609

610 Arculus, R.J., Ishizuka, O., Bogus, K., & the Expedition 351 Scientists (2015). *Proceedings*
611 *of the International Ocean Discovery Program, Expedition 351: Izu-Bonin-Mariana Arc*
612 *Origins:* College Station, TX (International Ocean Discovery Program).
613 https://doi.org/10.14379/iodp.proc.351.2015

614 Brown, M., Donadini, F., Nilsson, A., Panovska, S., Frank, U., Korhonen, K., Schuberth, M.,
615 Korte, M., & Constable, C. (2015). GEOMAGIA50.v3: 2. A new paleomagnetic database
616 for lake and marine sediments, *Earth, Planets and Space*, 67, 70.
617 https://doi.org/10.1186/s40623-015-0233-z

618 Channell, J.E.T., Xuan, C., & Hodell, D.A. (2009). Stacking paleointensity and oxygen
619 isotope data for the last 1.5 Myr (PISO-1500), *Earth and Planetary Science Letters*,
620 283, 14–23. https://doi.org/10.1016/j.epsl.2009.03.012

621 Constable, C., & Parker, R. (1991). Deconvolution of longcore palaeomagnetic
622 measurements - Spline therapy for the linear problem, *Geophysical Journal International*,
623 104, 453–468. https://doi.org/10.1111/j.1365-246X.1991.tb05693.x

624 Dodson, R. E., Fuller, M.D., & Pilant, W. (1974). On the measurement of the remanent
625 magnetism of long cores, *Geophysical Research Letters*, 1, 185–188.
626 https://doi.org/10.1029/GL001i004p00185

627 Guyodo, Y., Channell, J.E.T., & Thomas, R.G. (2002). Deconvolution of u-channel
628 paleomagnetic data near geomagnetic reversals & short events, *Geophysical Research*
629 *Letters*, 29, 1845. https://doi.org/10.1029/2002GL014927

630 Lascu, I., Jackson, M., & Solheid, P. (2012). Beyond U-channels, *IRM Quarterly*, 22, 1, 8-11.

631 Jackson, M., Bowles, J.A., Lascu, I., & Solheid, P. (2010). Deconvolution of u channel
632 magnetometer data: Experimental study of accuracy, resolution, and stability of different

633 inversion methods, *Geochemistry, Geophysics, Geosystems*, 11, Q07Y10.
634 https://doi.org/10.1029/2009GC002991
635 Korte, M., Constable, C., Donadini, F., & Holme, R. (2011). Reconstructing the Holocene
636 geomagnetic field, *Earth and Planetary Science Letters*, 312, 497–505.
637 https://doi.org/10.1016/j.epsl.2011.10.031
638 Nilsson, A., Holme, R., Korte, M., Suttie, N., & Hill, M. (2014). Reconstructing Holocene
639 geomagnetic field variation: new methods, models and implications, *Geophysical Journal*
640 *International*, 198, 229–248. https://doi.org/10.1093/gji/ggu120
641 Oda, H., & Shibuya, H. (1996). Deconvolution of long-core paleomagnetic data of Ocean
642 Drilling Program by Akaike's Bayesian Information Criterion minimization, *Journal of*
643 *Geophysical Research*, 101, 2815–2834. https://doi.org/10.1029/95JB02811
644 Oda, H., & Xuan, C. (2014). Deconvolution of continuous paleomagnetic data from pass-
645 through magnetometer: A new algorithm to restore geomagnetic and environmental
646 information based on realistic optimization, *Geochemistry, Geophysics, Geosystems*,15,
647 3907-3924. https://doi.org/10.1002/2014GC005513
648 Oda, H., Xuan, C., & Yamamoto, Y. (2016). Toward robust deconvolution of pass-through
649 paleomagnetic measurements: new tool to estimate magnetometer sensor response and
650 laser interferometry of sample positioning accuracy, *Earth, Planets and Space* , 68, 109.
651 https://doi.org/10.1186/s40623-016-0493-2
652 Parker, R.L., & Gee, J.S. (2002). Calibration of the pass-through magnetometer-II.
653 Application, *Geophysical Journal International*, 150, 140–152.
654 https://doi.org/10.1046/j.1365-246X.2002.01692.x
655 Philippe, É., Valet, J., St-Onge, G., & Thevarasan, A. (2018). Are Paleomagnetic Records
656 From U-Channels Appropriate for Studies of Reversals and Excursions?, *Geochemistry,*
657 *Geophysics, Geosystems*, 19, 4130–4142. https://doi.org/10.1029/2018GC007803

Roberts, A.P. (2006). High-resolution magnetic analysis of sediment cores: Strengths, limitations and strategies for maximizing the value of long-core magnetic data, *Physics of the Earth and Planetary Interiors*, 156, 162–178. https://doi.org/10.1016/j.pepi.2005.03.021

Roberts, A.P., Tauxe, L., & Heslop, D. (2013). Magnetic paleointensity stratigraphy and high-resolution Quaternary geochronology: successes and future challenges, *Quaternary Science Reviews*, 61, 1-16. https://doi.org/10.1016/j.quascirev.2012.10.036

Shibuya, H., & Michikawa, T. (2000). Calculation of superconducting rock magnetometer response, *Kumamoto Journal of Science (Earth Sciences)*, 16, 1–16.

Tauxe, L., Labrecque, J. L., Dodson, D., & Fuller, M. (1983). "U"channels - a new technique for paleomagnetic analysis of hydraulic piston cores, *EOS, Transactions, American Geophysical Union*, 64, 219.

Weeks, R., Laj, C., Endignoux, L., Fuller, M., Roberts, A., Manganne, R., Blanchard, E., & Goree, W. (1993). Improvements in long-core measurement techniques: Applications in palaeomagnetism and palaeoceanography, *Geophysical Journal International*, *114*, 651–662. https://doi.org/10.1111/j.1365-246X.1993.tb06994.x

Xuan, C., & Channell, J.E.T. (2009). UPmag: MATLAB software for viewing and processing u channel or other pass-through paleomagnetic data, *Geochemistry, Geophysics, Geosystems*, 10, Q10Y07. https://doi.org/10.1029/2009GC002584

Xuan, C., & Oda, H. (2015). UDECON: deconvolution optimization software for restoring high-resolution records from pass-through paleomagnetic measurements, *Earth, Planets and Space*, 67, 183. https://doi.org/10.1186/s40623-015-0332-x

Yamamoto, Y., Yamazaki, T., & Kanamatsu, T. (2018). An initial case study to deconvolve natural remanent magnetization of a continuous paleomagnetic sample using the software

UDECON, *Earth, Planets and Space*, 70, 160. https://doi.org/10.1186/s40623-018-0931-4

Figure Captions

Figure 1. Coordinates of SRM systems at University of Southampton and magnetic point source (MPS) cube and measurement blocks used for SRM sensor response estimate. (a) Photo of the old liquid-helium cooled SRM (SRM-old) and the new liquid-helium free SRM (SRM-new) inside a magnetically shielded room with orientation of the three orthogonal measurement axes indicated by arrows, (b) sketch of the SRM system from a side view, and (c) MPS sample cube and the two types of MPS measurement blocks used in this study. The MPS measurement block on the left has 5×5 grids with 5 mm spacing, and the measurement block on the right has 4×4 grids with 6 mm spacing.

Figure 2. (a) Magnetic moment of MPS-11 over time, and (b) deviation in sensitivities of the two SRMs at University of Southampton relative to ASPIN-2 spinner magnetometer at AIST. Black circles in (a) are magnetic moments measured on spinner magnetometer after sensitivity correction (see Table S1). Red dotted line in (a) is a sigmoidal curve fitted to the spinner magnetometer data using non-linear least squares regression. Magnetic moment of MPS-11 after sensitivity correction was 5.300×10^{-4} emu in Jan. 2016 and 5.244×10^{-4} emu in Oct. 2017 and Mar. 2018 (vertical dashed lines). Red and blue circles are magnetic moments measured on SRM-old and SRM-new, respectively. These values are averages of peak magnetic moments in X-, Y-, and Z-axis after integrating over a volume of $1\times1\times1$ cm^3 with cross-section centered in that of a u-channel (11.5 mm above the surface of the tray). Measurements on SRM-old in Dec. 2013 were conducted using MPS-2, which has an

estimated magnetic moment of 5.937×10^{-3} emu based on ASPIN-2 spinner magnetometer measurement after sensitivity correction (see Table S2). Orange and green horizontal lines are averages for SRM-old and SRM-new data, respectively.

Figure 3. Illustration of new approach for SRM sensor response estimate using MPS measurement data. The new approach allows sensor response to be estimated for measurements with varying sample cross-section shape (i.e. different integration volume width and height) and resolution along the Z-axis (i.e. integration volume length). Known difference between the center positions of the sample (black dot) and the MPS measurement grids (red dot) on cross-section is taken into account for more accurate sensor response estimate. The example shows the 3D interpolated (at 1mm intervals along all three axes) magnetic moment of the ZZ term measured using MPS-2 on SRM-old with a 5×5 grids MPS measurement block (see Figure 1c). Note that only results between 205-295 mm measurement positions along the Z-axis are shown. The MPS sample was placed at 250 mm position.

Figure 4. Screen captures of the URESPONSE software user interface. (a) An example of the software showing MPS measurements along three axes at multiple grid positions on cross-section. Selection of single or multiple runs of MPS measurement data can be done in the 'Measurement' panel, and users can choose to show any combinations of the X, Y, or Z-axis data using checkboxes in the 'Terms' panel. (b) An example of the software interface showing one of the estimated SRM sensor responses. The estimated sensor response is based on interpolation at 0.1 cm intervals followed by integration at 1-cm intervals along the Z-axis and over a 1.9×1.8 cm^2 cross-section area (red rectangle) using default response estimate

parameters. Users can choose to show any combinations of the nine response terms using checkboxes in the 'Terms' panel.

Figure 5. Sensor response estimates for SRM-old (a-d) and SRM-new (e-g) calculated by the URESPONSE software based on multiple sets of measurements using two MPS samples and following different measurement procedures (see Table 1). All calculations used the default response estimate parameters in the URESPONSE software. Normalization was made with the average of peak values in X and Y axes. Estimates in (a) and (b) used 1-mm resolution measurements of MPS-2 on SRM-old at 5×5 cross-section grid positions with MPS sample oriented parallel and antiparallel to measurement axes, respectively. Estimates in (c) and (d) used measurements of MPS-11 on SRM-old made at different time following the same procedures (i.e. both were collected at 2-mm interval resolution and using 4×4 cross-section grids). Estimates in (f) and (g) used MPS-11 measurements made on SRM-new at different time following the same procedures used for (c) and (d). Estimate in (e) used measurements on MPS-11 collected following the procedure similar to (f) and (g) but at every 10-mm resolution. Note that MPS-11 measurements used for (e) experienced drifting issues on X-axis at the time (right after SRM-new installation in Sept 2017), and hence any measurements along the X-axis were not used for sensor response estimate in (e). The full widths at half maximum (FWHM) and effective lengths (EL) for the three measurement axes are shown for each sensor response estimate.

Figure 6. Sensor response estimates for SRM-old (a-c) and SRM-new (d-f) calculated by the URESPONSE software using different sample geometry on cross-section and normalized with the calibrated magnetic moment value of MPS-11 (see Figure 2a): (a, d) a default 1.9×1.8 cm^2 area with 0 horizontal offset and 1 mm vertical offset from the grid center, (b, e)

a 1×1.8 cm^2 area with 0 horizontal offset and 5.5 mm vertical offset from the grid center, and (c, f) a 1.9×1.8 cm^2 area with -2 mm horizontal offset and 1 mm vertical offset from the grid center. All estimates used measurement data collected during the same time period (i.e. Oct. 2017) following the same procedures (see Table 1). SRM-old (a-c) and SRM-new (d-f) response estimates are based on the same MPS measurement data used for SRM-old_Est4 (see Figure 5d) and SRM-new_Est2 (see Figure 5f), respectively.

Figure 7. Differences between sensor response estimates shown in Figures 5 and 6 for (a) SRM-old and (b) SRM-new, and histograms of the differences in response estimates for (c) SRM-old and (d) SRM-new. All nine response terms are compared. SRM-old_Est4 (Figure 5d) and SRM-new_Est2 (Figure 5f) were subtracted from other response estimates in Figures 5 for SRM-old and SRM-new, respectively. To show difference caused by normalization method, SRM-old_Est4 and SRM-new_Est2 were subtracted from SRM-old_Est4_v2 (Figure 6a) and SRM-new_Est2_v2 (Figure 6b), respectively. SRM-old_Est4_v2 and SRM-new_Est2_v2 were subtracted from other response estimates for SRM-old and SRM-new shown in Figure 6, respectively. Standard deviations of response estimate difference curves in (a) and (b) are shown together with the keys for curves. Curves in (a) and (c) share the same key, and curves in (b) and (d) share the same key.

Figure 8. Comparison of repeated measurements (ten times on each SRM) of a test u-channel sample along three measurement axes on both SRM-old and SRM-new (a) before, and after (b) single and (c) full effective length (EL) normalizations. (d) Deconvolved data from repeated SRM-old and SRM-new measurements. Black, dark gray and gray lines represent X-, Y- and Z-axis data from SRM-old, respectively. Blue, green and red dash dotted lines represent X-, Y- and Z-axis data from SRM-new, respectively. Note that each unique color or

line style on the figure represents a group of ten curves plotted together. Vertical gray bars are 10-cm 'leader' and 'trailer' intervals measured immediately before and after the sample. It is clear that data after full EL normalization from both SRMs are more comparable than those calculated using single EL normalization, especially for X- and Y-axis data. Furthermore, deconvolution results of data from the two SRMs all show clearly enhanced variabilities and are highly consistent with one another.

Figure 9. Comparison of a test u-channel sample (a) declination, (b) inclination, and (c) total magnetization data from both SRM-old and SRM-new. Note that each unique color and line style on the figure represent a group of ten curves plotted together. Data shown are based on single and full EL normalized magnetization data as well as deconvolved data from both SRMs (i.e. Figures 8b-d). The two normalization methods yield small differences for data acquired on SRM-new, but declination data acquired on SRM-old using single and full EL normalization show differences up to ~10°. Deconvolution of SRM-old and SRM-new measurements are done in the UDECON software (Xuan & Oda, 2015) using SRM-old_Est4_v2 and SRM-new_Est2_v2, respectively. Deconvolution data from the two SRMs are remarkably similar and show clearly reproducible high-resolution features that are absent in the measurement data.

Figure 10. Comparison of deconvolution data of SRM-old (a-c) and SRM-new (d-f) measurements calculated using different sensor response estimates. Top, middle, and bottom plots are deconvolution data of X-, Y-, and Z-axis measurements, respectively. For data from each SRM, four sets of response estimates (all normalized by MPS magnetic moment) were used for deconvolution including the three sets of response estimates shown in Figure 6 and a set of response estimate that ignores all six cross-terms. Using inaccurate response estimates

for deconvolution appears to cause significant differences in the deconvolution results, especially for data from SRM-old.

Table 1. Summary of magnetic point source (MPS) measurements conducted on the old liquid-helium cooled SRM (SRM-old) and the new liquid-helium free SRM (SRM-new) at the University of Southampton.

MPS Sample	SRM	Measurement Grids on Cross-Section	Measurement Resolution (along track)	MPS Orientation	Measurement Date	Calculated Response Estimates
MPS-2	SRM-old	5×5 (5mm spacing)	1 mm	+X, +Y, or +Z	Dec. 2013	SRM-old_Est1
MPS-2	SRM-old	5×5 (5mm spacing)	1 mm	-X, -Y, or -Z	Dec. 2013	SRM-old_Est2
MPS-11	SRM-old	4×4 (6mm spacing)	2 mm	+X, +Y, or +Z	Jan. 2016	SRM-old_Est3
MPS-11	SRM-old	4×4 (6mm spacing)	2 mm	+X, +Y, or +Z	Oct. 2017	SRM-old_Est4
MPS-11	SRM-new	4×4 (6mm spacing)	10 mm	+X, +Y, or +Z	Sept. 2017	SRM-new_Est1
MPS-11	SRM-new	4×4 (6mm spacing)	2 mm	+X, +Y, or +Z	Oct. 2017	SRM-new_Est2
MPS-11	SRM-new	4×4 (6mm spacing)	2 mm	+X, +Y, or +Z	Mar. 2018	SRM-new_Est3

Figure 1.

(a) SRMs at the University of Southampton

(b) SRM system side view

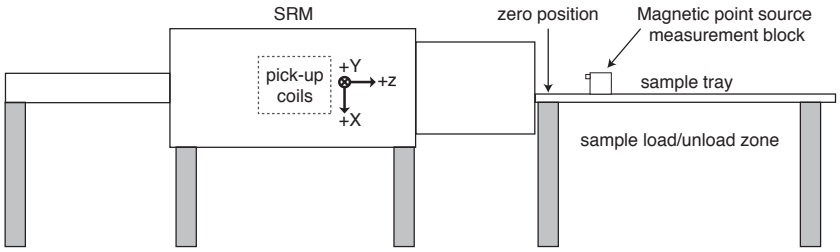

(c) Magnetic point source measurement blocks

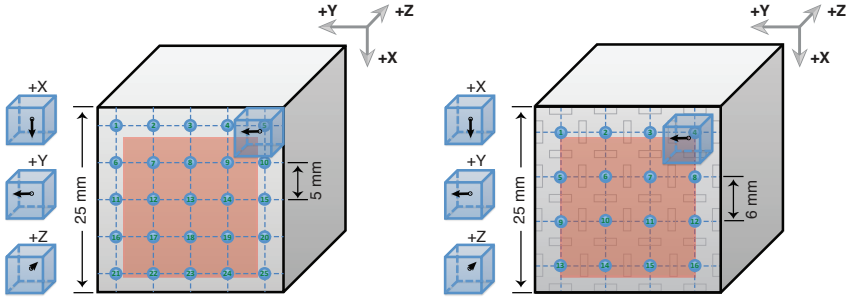

Figure 2.

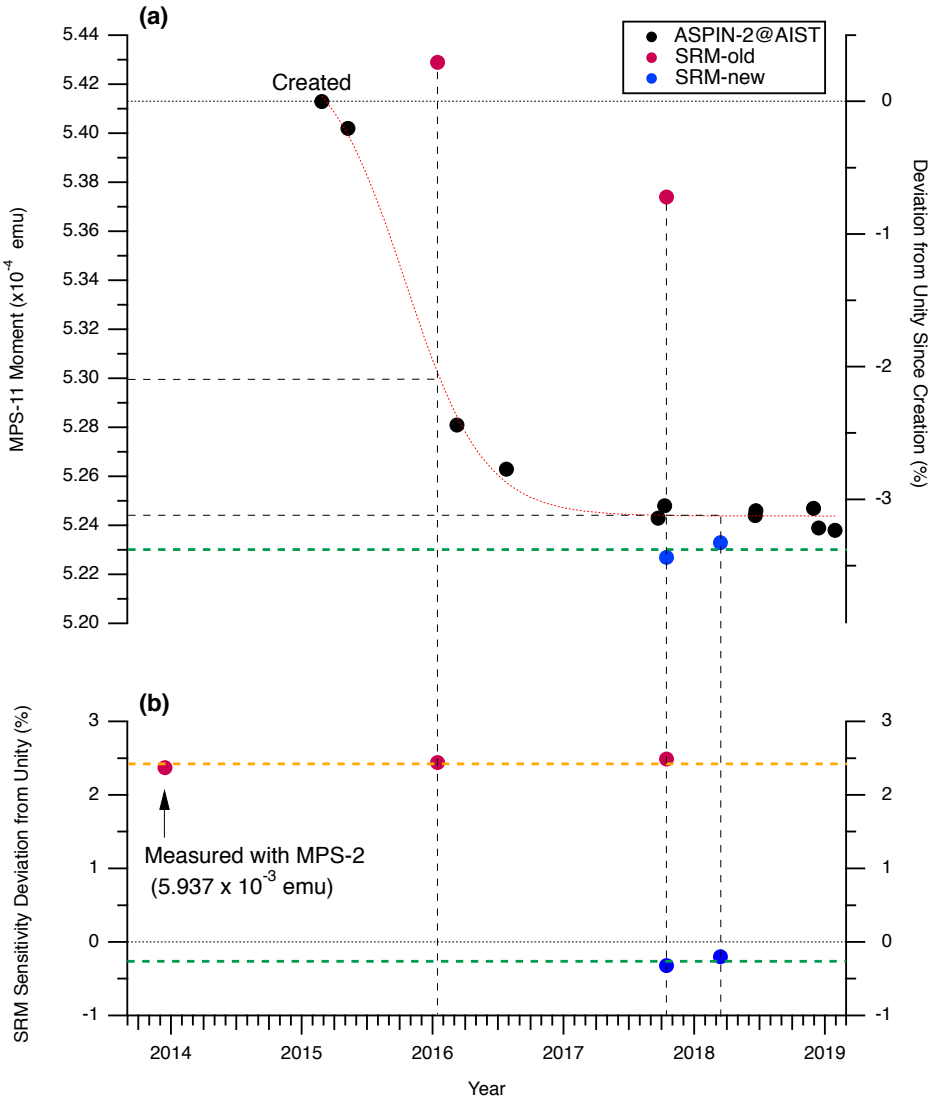
(a)
ASPIN-2@AIST
SRM-old
SRM-new
Created
MPS-11 Moment (x10^{-4} emu)
Deviation from Unity Since Creation (%)
5.44
5.42
5.40
5.38
5.36
5.34
5.32
5.30
5.28
5.26
5.24
5.22
5.20
0
-1
-2
-3
(b)
SRM Sensitivity Deviation from Unity (%)
Measured with MPS-2
(5.937 x 10^{-3} emu)
3
2
1
0
-1
2014
2015
2016
2017
2018
2019
Year

Figure 3.

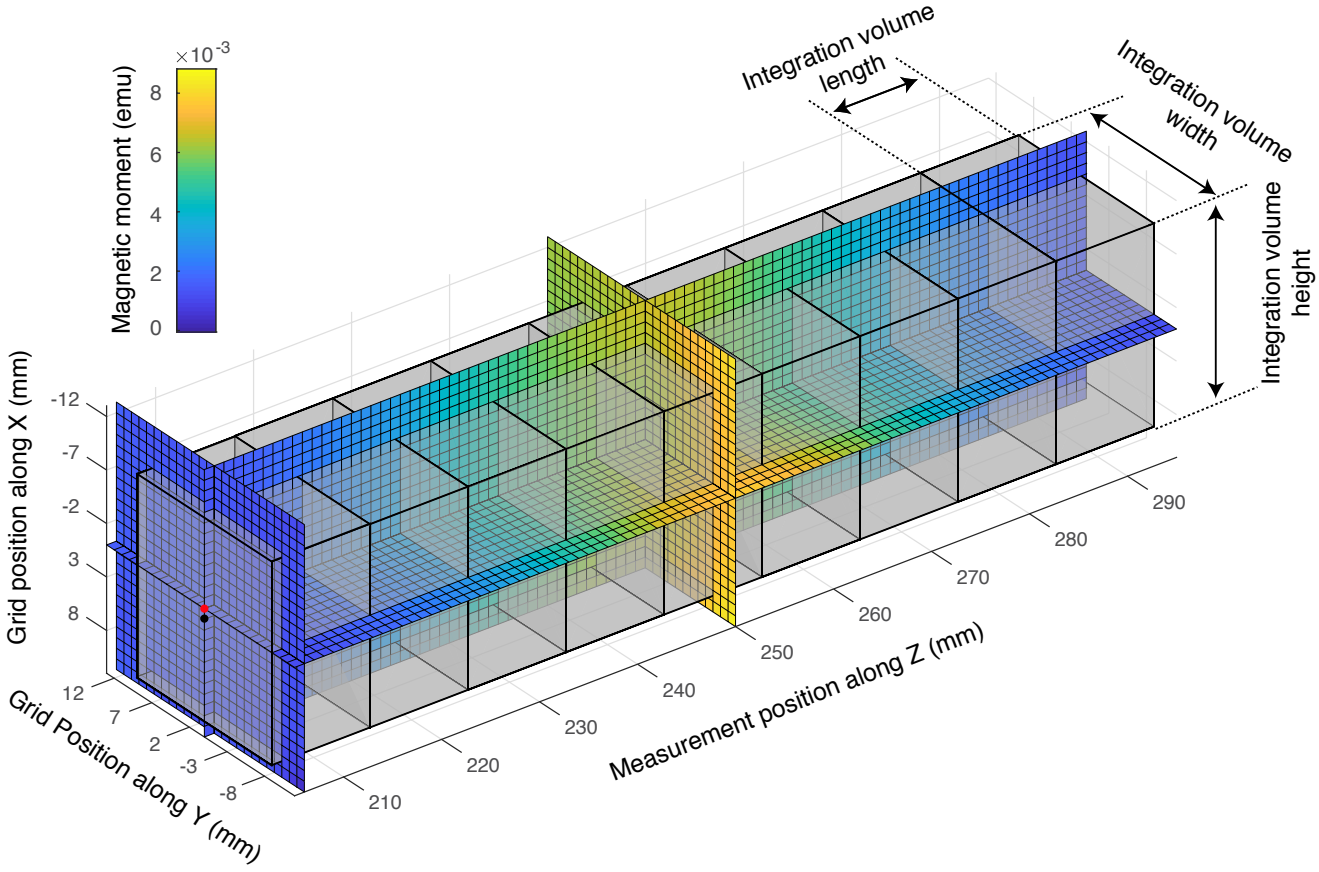
×10^-3
8
6
4
2
0
Magnetic moment (emu)
Integration volume length
Integration volume width
Integration volume height
Grid position along X (mm)
-12
-7
-2
3
8
Grid Position along Y (mm)
12
7
2
-3
-8
Measurement position along Z (mm)
210
220
230
240
250
260
270
280
290

Figure 4.

(a)

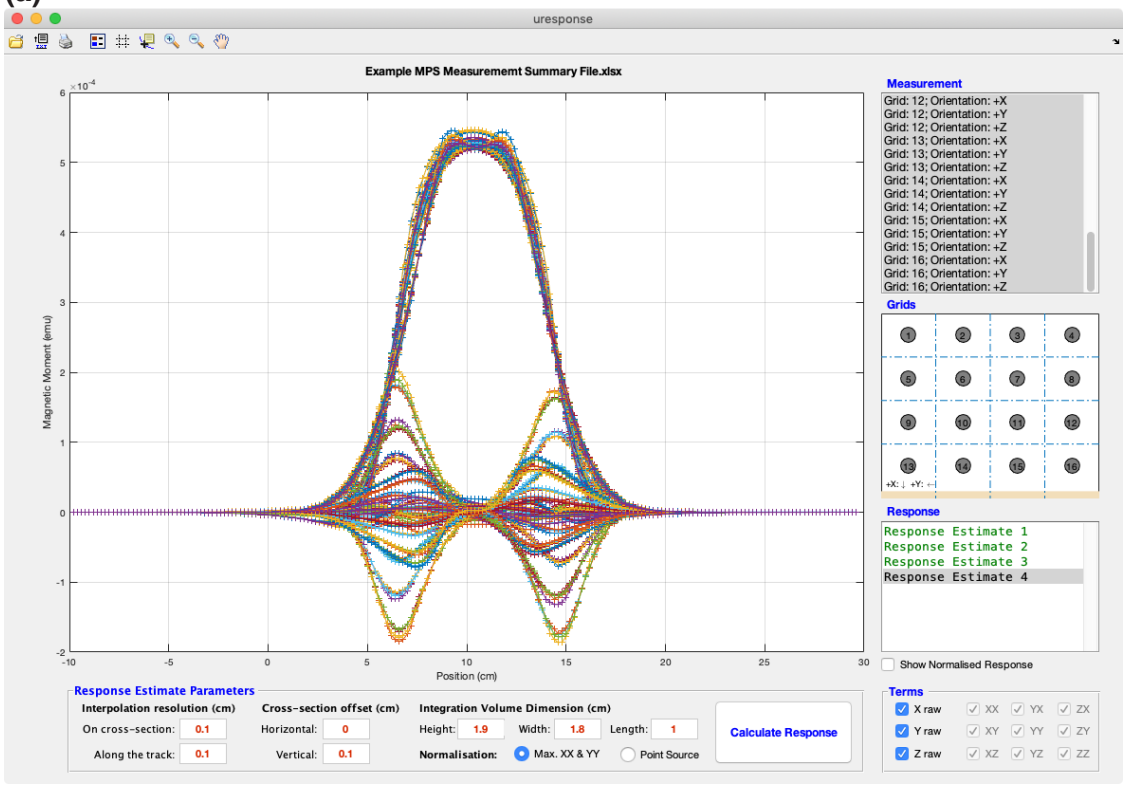
uresponse
Example MPS Measurememt Summary File.xlsx
Magnetic Moment (emu)
Position (cm)
Measurement
Grid: 12; Orientation: +X
Grid: 12; Orientation: +Y
Grid: 12; Orientation: +Z
Grid: 13; Orientation: +X
Grid: 13; Orientation: +Y
Grid: 13; Orientation: +Z
Grid: 14; Orientation: +X
Grid: 14; Orientation: +Y
Grid: 14; Orientation: +Z
Grid: 15; Orientation: +X
Grid: 15; Orientation: +Y
Grid: 15; Orientation: +Z
Grid: 16; Orientation: +X
Grid: 16; Orientation: +Y
Grid: 16; Orientation: +Z
Grids
Response
Response Estimate 1
Response Estimate 2
Response Estimate 3
Response Estimate 4
Show Normalised Response
Response Estimate Parameters
Interpolation resolution (cm)
On cross-section: 0.1
Along the track: 0.1
Cross-section offset (cm)
Horizontal: 0
Vertical: 0.1
Integration Volume Dimension (cm)
Height: 1.9
Width: 1.8
Length: 1
Normalisation: Max. XX & YY
Point Source
Calculate Response
Terms
X raw
Y raw
Z raw
XX
XY
XZ
YX
YY
YZ
ZX
ZY
ZZ

(b)

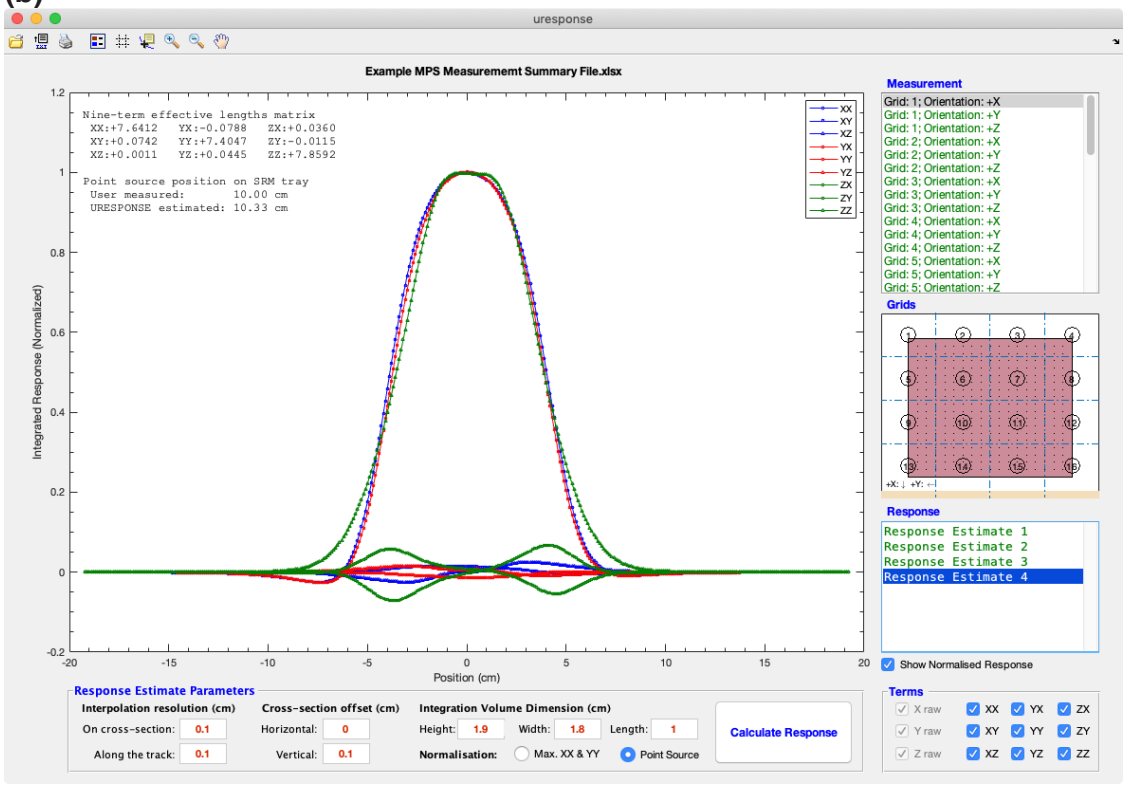
uresponse
Example MPS Measurememt Summary File.xlsx
Nine-term effective lengths matrix
XX:+7.6412 YX:-0.0788 ZX:+0.0360
XY:+0.0742 YY:+7.4047 ZY:-0.0115
XZ:+0.0011 YZ:+0.0445 ZZ:+7.8592
Point source position on SRM tray
User measured: 10.00 cm
URESPONSE estimated: 10.33 cm
Integrated Response (Normalized)
Position (cm)
Measurement
Grid: 1; Orientation: +X
Grid: 1; Orientation: +Y
Grid: 1; Orientation: +Z
Grid: 2; Orientation: +X
Grid: 2; Orientation: +Y
Grid: 2; Orientation: +Z
Grid: 3; Orientation: +X
Grid: 3; Orientation: +Y
Grid: 3; Orientation: +Z
Grid: 4; Orientation: +X
Grid: 4; Orientation: +Y
Grid: 4; Orientation: +Z
Grid: 5; Orientation: +X
Grid: 5; Orientation: +Y
Grid: 5; Orientation: +Z
Grids
Response
Response Estimate 1
Response Estimate 2
Response Estimate 3
Response Estimate 4
Show Normalised Response
Response Estimate Parameters
Interpolation resolution (cm)
On cross-section: 0.1
Along the track: 0.1
Cross-section offset (cm)
Horizontal: 0
Vertical: 0.1
Integration Volume Dimension (cm)
Height: 1.9
Width: 1.8
Length: 1
Normalisation: Max. XX & YY
Point Source
Calculate Response
Terms
X raw
Y raw
Z raw
XX
XY
XZ
YX
YY
YZ
ZX
ZY
ZZ

Figure 5.

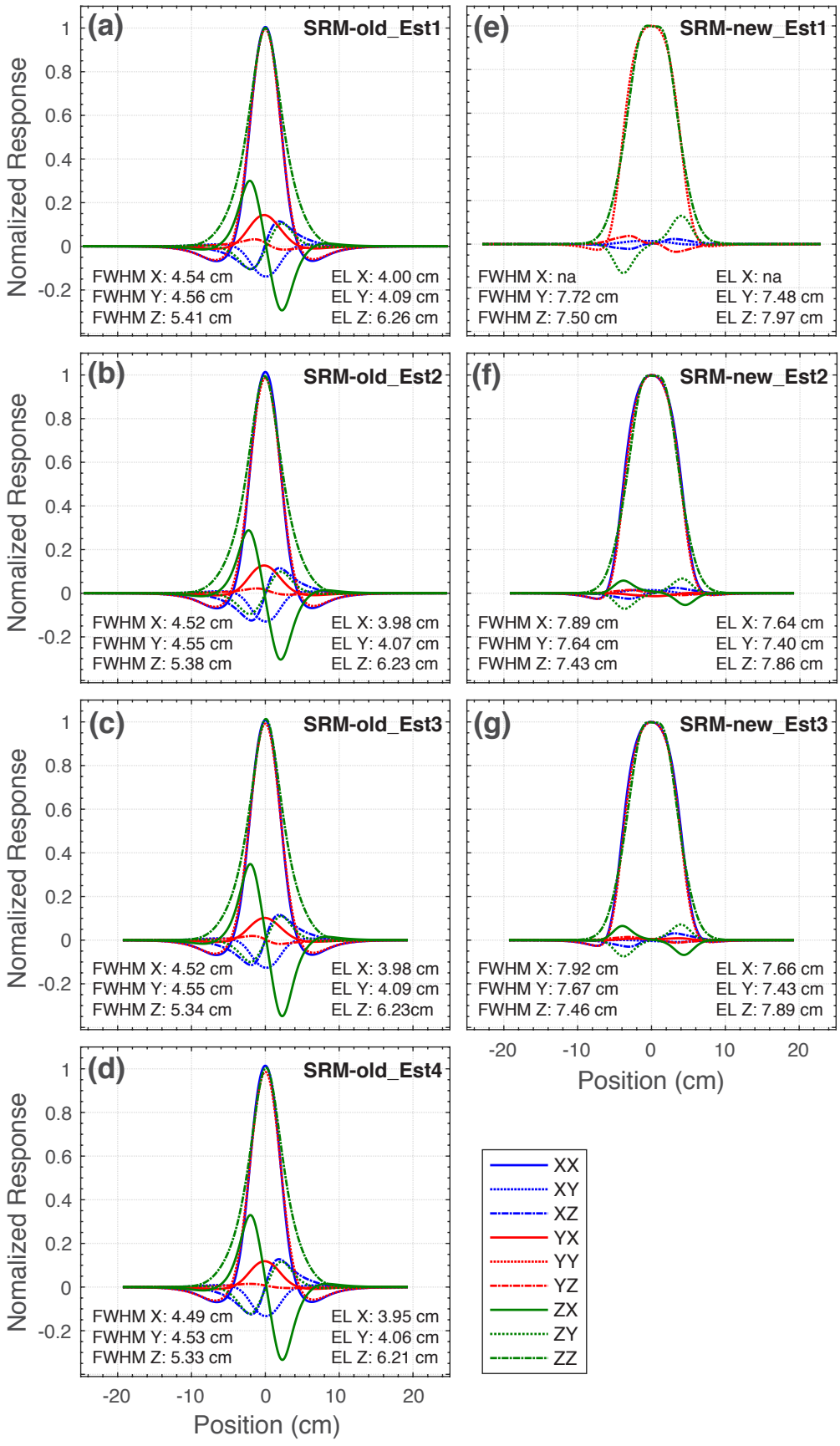
(a)
SRM-old_Est1
FWHM X: 4.54 cm
FWHM Y: 4.56 cm
FWHM Z: 5.41 cm
EL X: 4.00 cm
EL Y: 4.09 cm
EL Z: 6.26 cm
(e)
SRM-new_Est1
FWHM X: na
FWHM Y: 7.72 cm
FWHM Z: 7.50 cm
EL X: na
EL Y: 7.48 cm
EL Z: 7.97 cm
(b)
SRM-old_Est2
FWHM X: 4.52 cm
FWHM Y: 4.55 cm
FWHM Z: 5.38 cm
EL X: 3.98 cm
EL Y: 4.07 cm
EL Z: 6.23 cm
(f)
SRM-new_Est2
FWHM X: 7.89 cm
FWHM Y: 7.64 cm
FWHM Z: 7.43 cm
EL X: 7.64 cm
EL Y: 7.40 cm
EL Z: 7.86 cm
(c)
SRM-old_Est3
FWHM X: 4.52 cm
FWHM Y: 4.55 cm
FWHM Z: 5.34 cm
EL X: 3.98 cm
EL Y: 4.09 cm
EL Z: 6.23cm
(g)
SRM-new_Est3
FWHM X: 7.92 cm
FWHM Y: 7.67 cm
FWHM Z: 7.46 cm
EL X: 7.66 cm
EL Y: 7.43 cm
EL Z: 7.89 cm
(d)
SRM-old_Est4
FWHM X: 4.49 cm
FWHM Y: 4.53 cm
FWHM Z: 5.33 cm
EL X: 3.95 cm
EL Y: 4.06 cm
EL Z: 6.21 cm
Nomalized Response
1
0.8
0.6
0.4
0.2
0
-0.2
-20
-10
0
10
20
Position (cm)
XX
XY
XZ
YX
YY
YZ
ZX
ZY
ZZ

Figure 6.

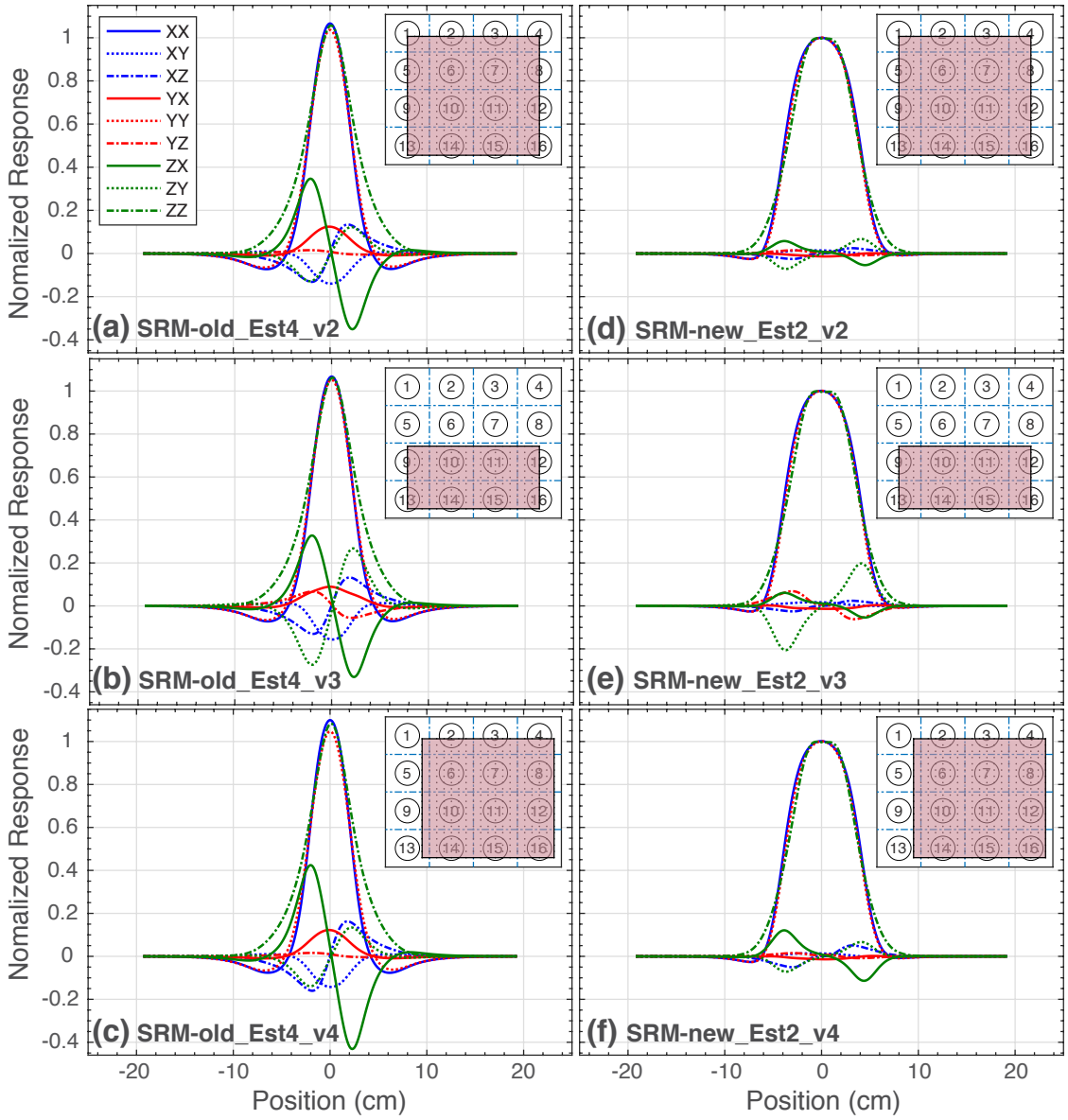
XX
XY
XZ
YX
YY
YZ
ZX
ZY
ZZ
Nomalized Response
Position (cm)
(a) SRM-old_Est4_v2
(b) SRM-old_Est4_v3
(c) SRM-old_Est4_v4
(d) SRM-new_Est2_v2
(e) SRM-new_Est2_v3
(f) SRM-new_Est2_v4

Figure 7.

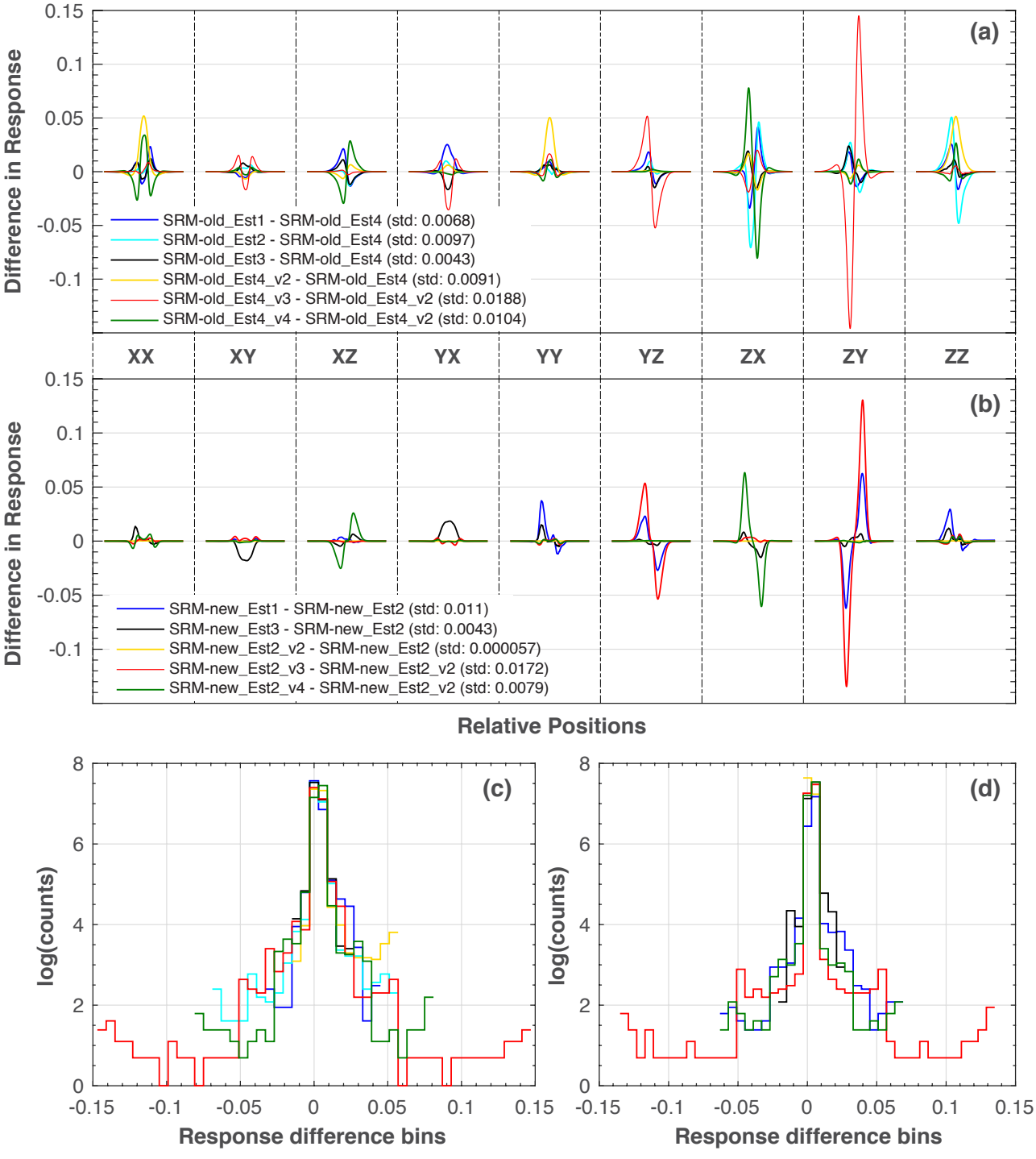
(a)
Difference in Response
0.15
0.1
0.05
0
-0.05
-0.1
SRM-old_Est1 - SRM-old_Est4 (std: 0.0068)
SRM-old_Est2 - SRM-old_Est4 (std: 0.0097)
SRM-old_Est3 - SRM-old_Est4 (std: 0.0043)
SRM-old_Est4_v2 - SRM-old_Est4 (std: 0.0091)
SRM-old_Est4_v3 - SRM-old_Est4_v2 (std: 0.0188)
SRM-old_Est4_v4 - SRM-old_Est4_v2 (std: 0.0104)
XX
XY
XZ
YX
YY
YZ
ZX
ZY
ZZ
(b)
Difference in Response
SRM-new_Est1 - SRM-new_Est2 (std: 0.011)
SRM-new_Est3 - SRM-new_Est2 (std: 0.0043)
SRM-new_Est2_v2 - SRM-new_Est2 (std: 0.000057)
SRM-new_Est2_v3 - SRM-new_Est2_v2 (std: 0.0172)
SRM-new_Est2_v4 - SRM-new_Est2_v2 (std: 0.0079)
Relative Positions
(c)
log(counts)
8
6
4
2
0
-0.15
-0.1
-0.05
0
0.05
0.1
0.15
Response difference bins
(d)
log(counts)
Response difference bins

Figure 8.

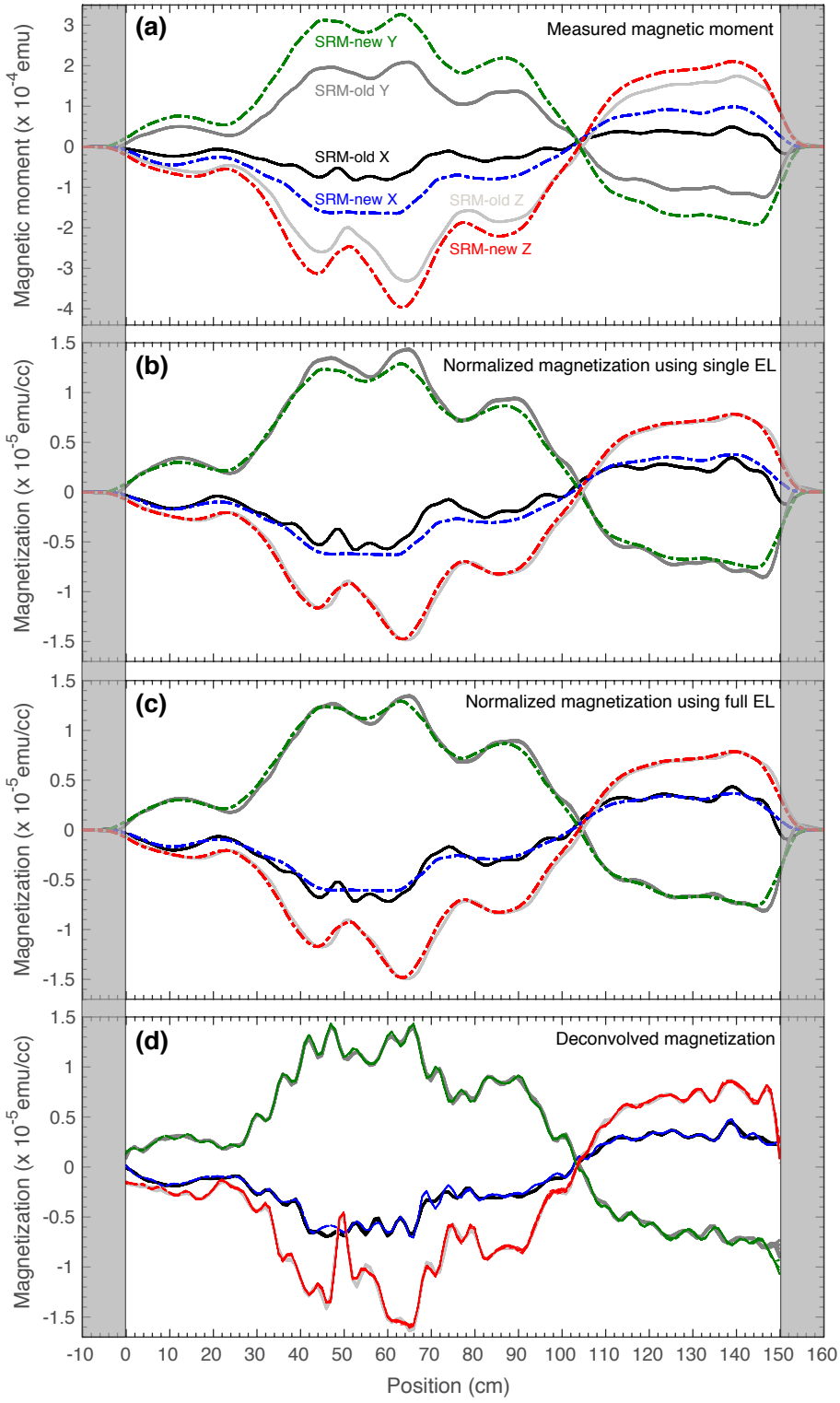
(a)
Measured magnetic moment
SRM-new Y
SRM-old Y
SRM-old X
SRM-new X
SRM-old Z
SRM-new Z
Magnetic moment (x 10^-4 emu)
(b)
Normalized magnetization using single EL
Magnetization (x 10^-5 emu/cc)
(c)
Normalized magnetization using full EL
Magnetization (x 10^-5 emu/cc)
(d)
Deconvolved magnetization
Magnetization (x 10^-5 emu/cc)
Position (cm)

Figure 9.

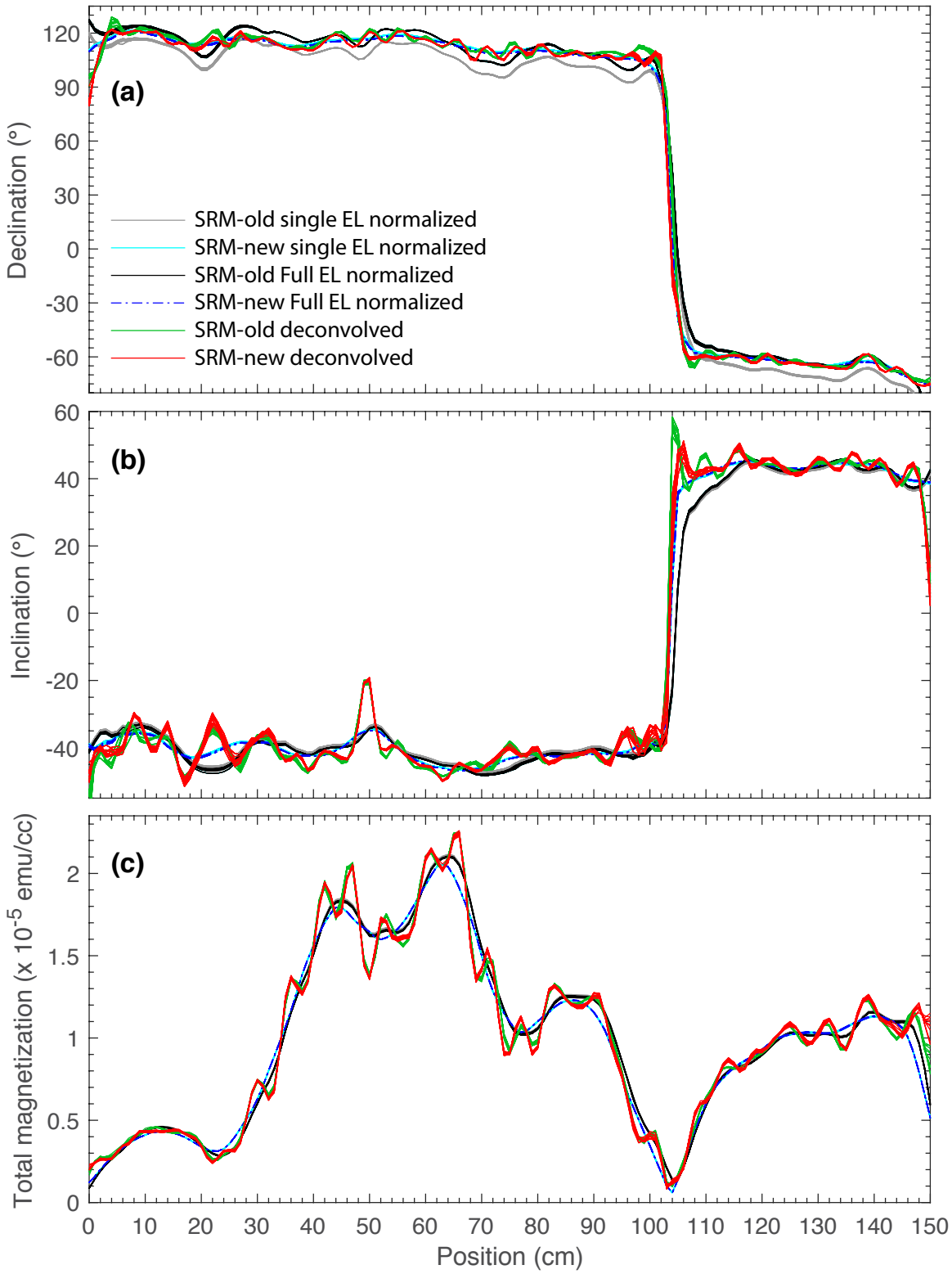
(a)
Declination (°)
120
90
60
30
0
-30
-60
SRM-old single EL normalized
SRM-new single EL normalized
SRM-old Full EL normalized
SRM-new Full EL normalized
SRM-old deconvolved
SRM-new deconvolved
(b)
Inclination (°)
60
40
20
0
-20
-40
(c)
Total magnetization (x 10-5 emu/cc)
2
1.5
1
0.5
0
0
10
20
30
40
50
60
70
80
90
100
110
120
130
140
150
Position (cm)

Figure 10.

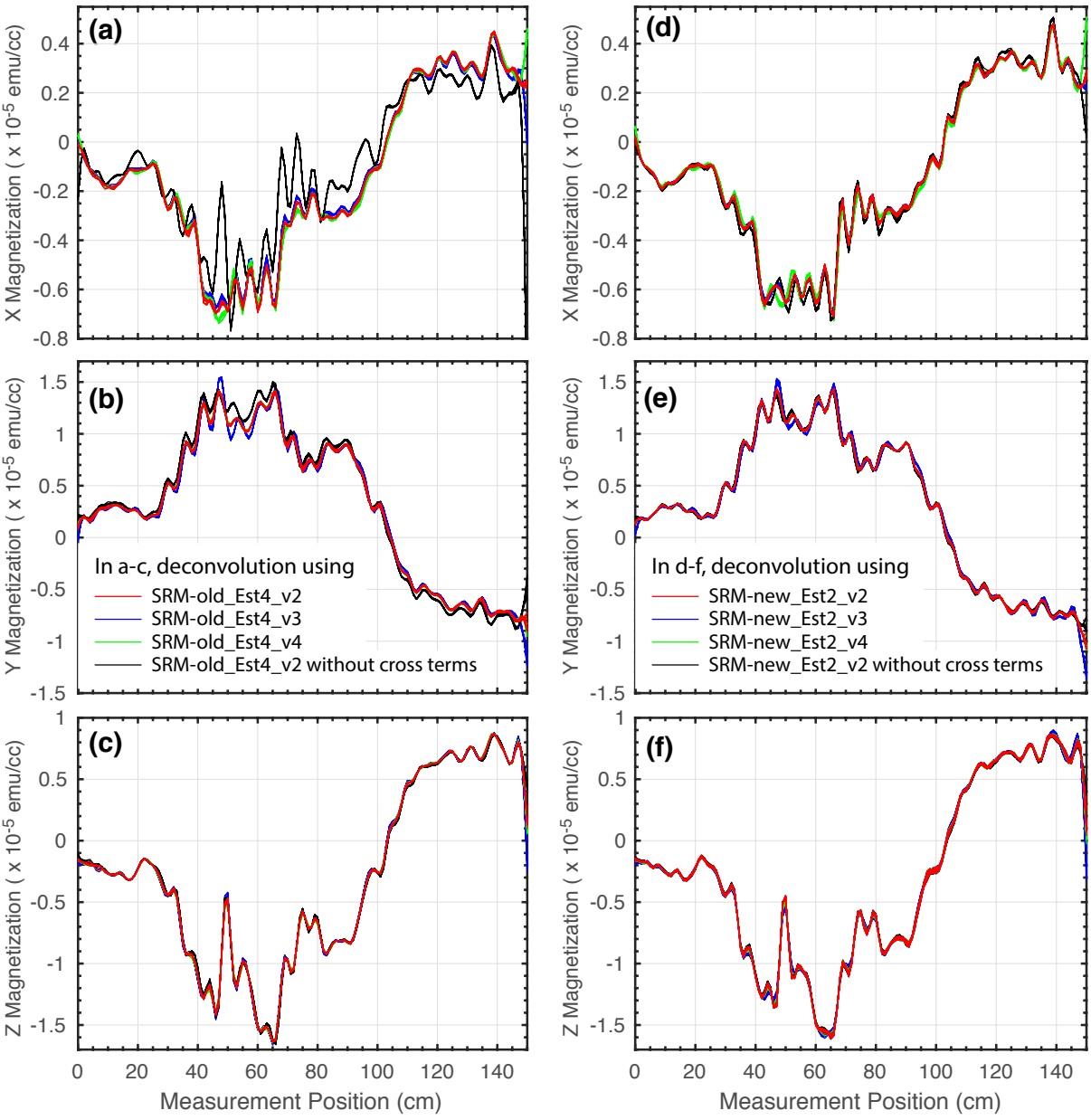
(a)
(b)
(c)
(d)
(e)
(f)
X Magnetization (x 10-5 emu/cc)
Y Magnetization (x 10-5 emu/cc)
Z Magnetization (x 10-5 emu/cc)
Measurement Position (cm)
In a-c, deconvolution using
SRM-old_Est4_v2
SRM-old_Est4_v3
SRM-old_Est4_v4
SRM-old_Est4_v2 without cross terms
In d-f, deconvolution using
SRM-new_Est2_v2
SRM-new_Est2_v3
SRM-new_Est2_v4
SRM-new_Est2_v2 without cross terms